

Experimental and atomistic theoretical study of degree of polarization from multilayer InAs/GaAs quantum dot stacks

Muhammad Usman,^{1,*} Tomoya Inoue,² Yukihiro Harda,² Gerhard Klimeck,³ and Takashi Kita²

¹*Tyndall National Institute, Lee Maltings, Dyke Parade, Cork, Ireland*

²*Department of Electrical and Electronic Engineering, Graduate School of Engineering, 1-1 Rokkodai, Nada, Kobe 657-8501, Japan*

³*Purdue University, Network for Computational Nanotechnology, Birck Nanotechnology Center, 1205 West State Street, West Lafayette, Indiana 47907, USA*

(Received 27 May 2011; published 23 September 2011)

Recent experimental measurements, without any theoretical guidance, showed that isotropic polarization response can be achieved by increasing the number of quantum-dot (QD) layers in a QD stack. Here we analyze the polarization response of multilayer QD stacks containing up to nine QD layers by linearly polarized photoluminescence (PL) measurements and by carrying out a systematic set of multimillion atom simulations. The atomistic modeling and simulations allow us to include correct symmetry properties in the calculations of the optical spectra, a factor critical to explain the experimental evidence. The values of the degree of polarization (DOP) calculated from our model follows the trends of the experimental data. We also present detailed physical insight by examining strain profiles, band edges diagrams, and wave function plots. Multidirectional PL measurements and calculations of the DOP reveal a unique property of InAs QD stacks that the TE response is anisotropic in the plane of the stacks. Therefore, a single value of the DOP is not sufficient to fully characterize the polarization response. We explain this anisotropy of the TE modes by orientation of hole-wave functions along the $[\bar{1}10]$ direction. Our results provide a new insight that isotropic polarization response measured in the experimental PL spectra is due to two factors: (i) TM_{001} -mode contributions increase due to enhanced intermixing of HH and LH bands, and (ii) TE_{110} -mode contributions reduce significantly due to hole-wave function alignment along the $[\bar{1}10]$ direction. We also present optical spectra for various geometry configurations of QD stacks to provide a guide to experimentalists for the design of multilayer QD stacks for optical devices. Our results predict that the QD stacks with identical layers will exhibit lower values of the DOP than the stacks with nonidentical layers.

DOI: [10.1103/PhysRevB.84.115321](https://doi.org/10.1103/PhysRevB.84.115321)

PACS number(s): 78.67.Hc, 73.22.Dj, 73.63.Kv, 78.60.Fi

I. INTRODUCTION

The atom-like density of states in semiconductor quantum dots is quite promising to design optical devices such as lasers, semiconductor optical amplifiers, etc., with high saturation powers and fast response. Recently, bilayer and multilayer quantum-dot (QD) stacks have attracted strong interests because of their operating wavelengths within the telecommunication range of interest (1.3–1.5 μm). However, for practical design of optical devices, polarization-insensitive optical spectra are needed. Therefore, controlling polarization response in QD systems is a critical issue.

The polarization response of QDs is measured in terms of DOP, defined as

$$\text{DOP} = \frac{TE_{\perp\text{-growth}} - TM_{\parallel\text{-growth}}}{TE_{\perp\text{-growth}} + TM_{\parallel\text{-growth}}} \quad (1)$$

Here $TE_{\perp\text{-growth}}$ refers to traverse electric mode in a direction perpendicular to the growth direction ($[001]$) and $TM_{\parallel\text{-growth}}$ refers to traverse magnetic mode along the growth direction ($[001]$). The value of DOP depends on the chosen direction for the TE mode in the plane of QD. While the previous studies of polarization response of QDs provide only one value of DOP corresponding to a chosen direction for the TE mode,^{1–4} we associate DOP with the direction of TE mode, for example $TE_{110} \rightarrow \text{DOP}_{110}$, $TE_{\bar{1}10} \rightarrow \text{DOP}_{\bar{1}10}$, $TE_{100} \rightarrow \text{DOP}_{100}$, and $TE_{010} \rightarrow \text{DOP}_{010}$, and show that the DOP depends highly on the chosen direction. Only one DOP value is not sufficient to fully characterize the polarization response of QD systems.

The InAs QDs obtained from the Stranski-Krastanov self-assembly growth process typically have a flat shape; that is, the base diameter is typically 4–5 times larger than the height. In such QDs, compressive biaxial strain splits the heavy hole (HH) and light hole (LH) bands by more than 100 meV. As a result, only the TE mode can couple and the TM mode is very weak.⁵ The polarization response of such systems is highly anisotropic, TE mode \gg TM mode and $\text{DOP} \rightarrow 1.0$. To achieve the desired isotropic response ($\text{DOP} = 0$) for the design of optical devices, significant tuning of QD geometry, band structure manipulation, and/or strain engineering are required.

During the last few years, several techniques have been explored to achieve polarization-insensitive optical emission from InAs QD samples. These methods include overgrowing the InAs QD samples by an InGaAs strain-relaxing capping layer (SRCL),^{6,7} growing large stacks of QDs in the form of columnar QDs,^{1,2,8,9} bilayer,¹⁰ trilayer QD,¹¹ multilayer stacks,^{3,12,13} and band-gap engineering by including dilute nitrogen N (Ref. 14), phosphorous P (Ref. 15), and antimony Sb (Ref. 16) impurities. T. Kita *et al.*⁹ and T. Saito *et al.*² demonstrated that an isotropic polarization response can be obtained by growing columnar QDs consisting of nine QD layers.

Recent experiments by T. Inoue *et al.*^{3,17,18} showed, without any theoretical guidance, that similar tuning of polarization properties is possible in regular InAs QD stacks where the QD layers are geometrically separated by thin GaAs spacers. Such multilayer QD stacks have a twofold advantage over columnar

QDs: (i) A moderately thick GaAs spacer between the QD layers allows precise control of overall QD shape and size; (ii) reduced strain accumulation results in isotropic polarization response with fewer QD layers in the stack. The experimental results are provided for QD stacks containing three, six, and nine QD layers. The results indicate that the DOP_{110} takes up the values of $+0.46$ and -0.60 for the samples containing six and nine QD layers, respectively. A change of sign for the DOP_{110} implies that an isotropic polarization response ($DOP \sim 0$) can be achieved by engineering the number of QD layers in the stack.

The previous experimental measurements³ indicated a prospect to achieve polarization-insensitive response; however, no theoretical study is available to date to provide physical insight for the design of these complex multimillion atom nanostructures. Furthermore, the experiments only analyze TE_{110} mode, whereas PL measurements along multiple in-plane directions are required to fully characterize the polarization properties of these QD systems.

This article aims to thoroughly investigate the optical spectra of multilayer QD stacks by in-plane polarization measurements and atomistic theoretical analysis. Our PL measurements reveal unique properties of these QD stacks containing strongly coupled electronic states and the atomistic theory explains the experimental evidence very well. The modeling and simulations also provide data for DOP for different geometry configurations and in-plane directions for the TE mode to explore the design space and provide a guide for future experiments.

II. EXPERIMENTAL PROCEDURE

The QD samples are grown on an undoped [001] GaAs substrate using solid-source molecular-beam epitaxy. First a

thick layer of GaAs buffer layer is grown at 550°C , followed by repetitions of the InAs QD layers and GaAs spacer layers with growth interruptions of 10 s after each GaAs spacer layer reached a thickness of 16 ML. The nominal thickness of the InAs is kept at 1.9 ML. Finally, the QD layers are capped with a 100-nm-thick GaAs layer. Further details of our growth process can be found in earlier publications.^{3,17–19} The crystallographic properties of the stacked QDs are examined using a cross-sectional transmission electron microscope (TEM). The TEM images of the samples containing three, six, and nine QD layers are shown in Fig. 1(a).³

Next, we perform linearly polarized PL measurements at room temperature to investigate the polarization-dependent optical spectra. The laser diode excitation is at 659-nm wavelength. The detailed setup and measurement procedure is described by T. Inoue *et al.*¹⁷ The polarization-dependent PL spectra are shown in Fig. 1 for a single QD layer [panels (b)–(d)] and nine QD layers [panels (e)–(g)].

Figures 1(b)–1(d) indicate for a single QD that TE_{110} and $TE_{\bar{1}10}$ show a similar magnitude and that TM_{001} has a much smaller response than both in-plane TE modes. This is typical for InAs QDs and is due to the compressive biaxial strain that splits the HH-LH band edges, resulting in HH-type valence band states close to band gap. Previous theoretical and experimental studies on single QDs have shown similar properties.

The PL spectra in Figs. 1(e)–1(g), on the contrary, reveal an interesting and unique property of the InAs/GaAs QD stacks that the TE_{110} response is significantly less than the $TE_{\bar{1}10}$ response. No previous evidence exists for such TE-mode anisotropy in InAs/GaAs QDs, though Podemski *et al.*²⁰ have reported similar results for InP-based columnar quantum dash structures. The measured difference between the two TE modes is such that even the DOP for the same QD stack could

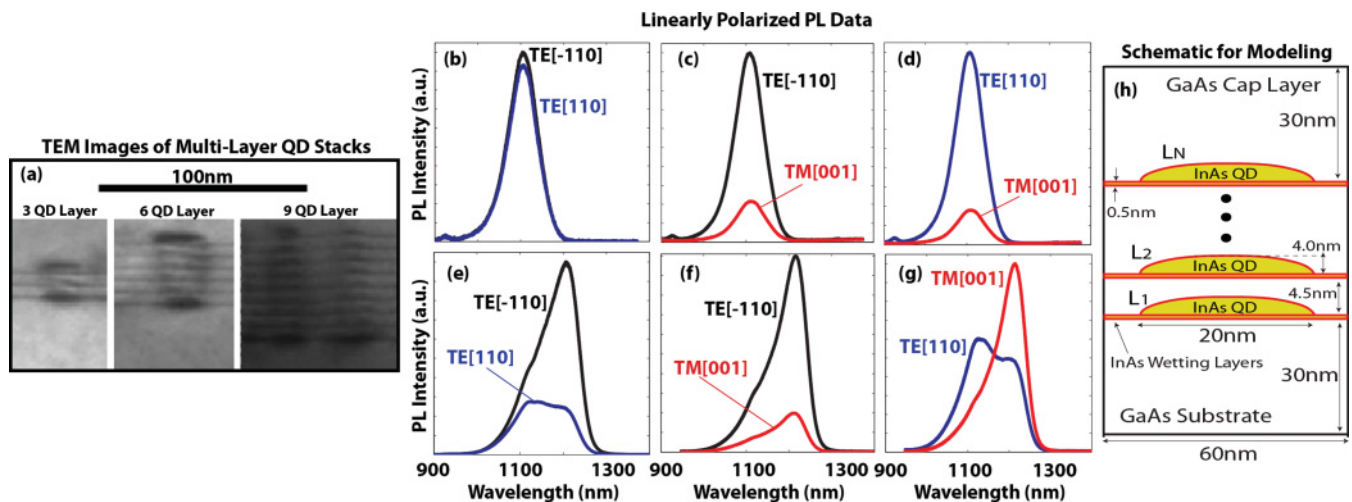


FIG. 1. (Color online) (a) TEM images of three-, six-, and nine-QD-layer stacks grown by solid-source molecular-beam epitaxy (Ref. 3). The layers of InAs QDs separated by GaAs intermediate layers are stacked with clear wetting layer interfaces. (b),(c),(d) Linearly polarized PL measurements for TE_{110} , $TE_{\bar{1}10}$, and TM_{001} modes for single QD layer. (e),(f),(g) Linearly polarized PL measurements for TE_{110} , $TE_{\bar{1}10}$, and TM_{001} modes for a nine-QD-layers sample. The PL plots in panels (b)–(g) are from independent experimental measurements. Each one of them is normalized to its highest peak. (h) The schematic diagram of the simulated system. InAs QD layers are embedded inside a GaAs buffer. Each layer consists of a dome-shaped QD on top of a 1.0-ML InAs wetting layer. QD layers are denoted by L_N , with N being the number of QD layers in the stack. The wetting layers are separated by a 4.5-nm GaAs buffer.

have different signs when measured along the $[110]$ and $[\bar{1}10]$ directions. The reason for such TE-mode anisotropy is highly nonintuitive and requires modeling and simulations of these large QD structures. The modeling must include the correct symmetry properties because the long-range strain affects the room-temperature material properties and atomistic structure resolution. The multimillion atom simulations presented in this article explain the experimental measurements in terms of hole-wave-function alignments along the $[\bar{1}10]$ direction.

III. THEORETICAL MODEL

The theoretical modeling of QD stacks containing up to nine QD layers possesses a twofold challenge: First, it requires an atomistic model that can calculate electronic and optical properties including correct symmetry and interfaces. Second, the large size of QD stacks requires calculations to be done over millions of atoms to properly include the long-range effects of strain. We use NEMO 3-D^{21,22} to analyze the electronic and optical properties of multilayer QD stacks. NEMO 3-D is based on fully atomistic calculations of strain and electronic structure: The strain is calculated by using the atomistic valence force field (VFF) model,²³ including anharmonic corrections²⁴ to the Keating potential, and the electronic structure is calculated by solving a Hamiltonian inside a 20-band $sp^3d^5s^*$ basis.²⁵

NEMO 3-D has been designed and optimized to be scalable from a single CPU to a large number of processors on the most advanced supercomputing clusters. Excellent MPI-based scaling to 8192 cores/CPU has been demonstrated.²⁶ The atomistic modeling techniques and parallel coding scheme implemented in NEMO 3-D allows it to simulate large QD stacks with realistic geometry extension and symmetry properties. Past NEMO 3-D-based studies of nanostructures include (i) single InAs QD with InGaAs SRCL,⁶ InAs bilayer QDs,^{10,27} and InAs multilayer QD stacks,²⁸ (ii) valley splitting in miscut Si quantum wells on SiGe substrate,²⁹ (iii) Stark effect of single P impurities in Si,³⁰ and (iv) dilute Bi impurities in GaAs and GaP materials.³¹

IV. SIMULATED SYSTEM

The theoretical analysis of the multilayer QD stacks containing up to nine layers is carried out through a set of systematic simulations. The geometry parameters of the QD samples are extracted from the TEM images shown in Fig. 1(a), which indicates that all the QDs in the stacks are of nearly identical size. Some topmost layers in the nine QD stack appear to be relatively small and are only partially grown.³ The schematic diagram of the system modeled in our simulations is shown in Fig. 1(h). Multiple QD layers separated by a 4.5-nm-thick GaAs buffer are embedded inside a large GaAs matrix. This wetting layer-to-layer separation is experimentally optimized to obtain uniform vertical QD stacks from the self-assembly growth process.¹⁷ Each QD layer consists of a dome-shaped InAs QD with a circular base, lying on top of a 1.0-ML InAs wetting layer. The QD systems with single, three, six, and nine QD layers will be labeled as L_1 , L_3 , L_6 , and L_9 , respectively.

The size of QDs extracted from the TEM images indicates a base diameter of ~ 20 nm and height of ~ 4 nm. Since

the height of the QDs in the TEM images is not very clear, we choose to simulate three different QD geometries in our theoretical study. (i) All QD layers are identical with 20 nm base diameter and 4 nm height of the QD in each layer. All the results presented are for this system unless other dimensions are specified. (ii) All QD layers are identical with 20 nm base diameter and 3.5 nm height of the QD in each layer. (iii) The size of QDs increases from the lower to the upper layers: The base diameter increases by 1 nm and the height increases by 0.25 nm. We choose this last system (iii) because past experiments of multilayer QD stacks^{10,32} have indicated an increasing size of QDs when multilayer QD stacks are grown by the self-assembly process, so it is interesting to theoretically investigate this geometry. We also simulate a system, L_9 , in which the height of QDs in each layer is 4.5 nm. This would mean that the top of each QD will be touching its upper adjacent wetting layer, approaching the columnar QD limit. The theoretical results presented here for various QD geometries provide a guide for experimentalists to understand the dependence of DOP on the QD geometry since experimental investigations of QD stacks for polarization response are still under way.

The QD layers are embedded inside a sufficiently large GaAs buffer to ensure proper relaxation of atoms and to accommodate the long-range effects of strain. The size of the largest GaAs buffer for the system containing nine QD layers, L_9 , is $60 \times 60 \times 106$ nm³, consisting of $\sim 24.4 \times 10^6$ atoms. Mixed boundary conditions are applied in the strain minimization: The substrate is fixed at the bottom, the GaAs matrix is periodic in lateral dimensions, and the capping layer is free to relax from the top. The electronic structure calculations use a separate subdomain with closed boundary conditions to reduce the computational burden,²² with a surface passivation³³ which avoids artificial surface states in the atomistic representation.

A. Electron wave functions form molecular states

Figure 2 shows the plots of the lowest conduction band state E_1 for all of the four QD systems under study. From the top views of the wave functions (second row), it is evident that the lowest electron state is of s -type symmetry. The side views of the wave functions (first row) show that the electron state forms a hybridized (molecular) state in L_3 , L_6 , and L_9 stacks and is spread over all of the QDs. This is due to strong coupling of QDs at 4.5-nm separation. The presence of the s -like electron wave function in all of the QDs implies that only the details of hole-wave functions inside the QD stack will determine the optical activity of a particular QD inside the stack. This is different from the previous study of bilayers,¹⁰ where a weak coupling of QDs at 10-nm separation resulted in atomic-like electron wave functions. In the bilayer system, both the electron and the hole-wave functions determined the optical activity of the QDs. Previous studies on the identical bilayer²⁷ and stacks with seven identical QDs²⁸ showed that the strain tends to push the electron states toward the lower QDs in such systems. The electron wave functions for L_3 and L_6 systems follow this trend. Here we find that this trend is no longer true for stacks with nine QD layers, L_9 , where the electron wave function E_1 vanishes around the edges of the

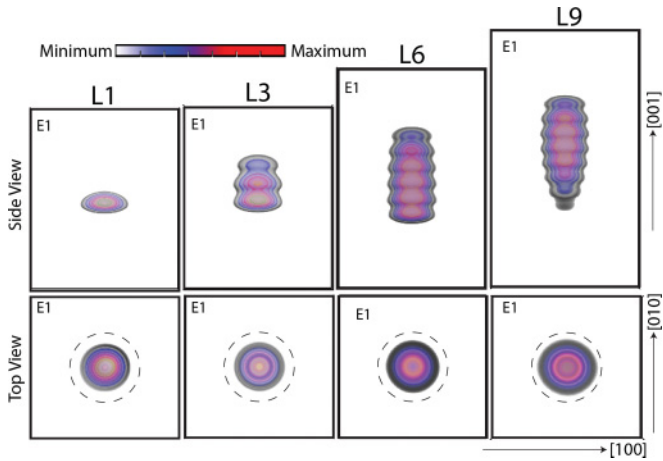


FIG. 2. (Color online) Plots of the lowest conduction band state, E_1 , for QD systems L_1 , L_3 , L_6 , and L_9 . (Top row) The side view of the plots. (Bottom row) The top view of the plots. The intensity of the color in the plots indicates the magnitude of the wave function: The red color represents the highest magnitude and the light blue color represents the lowest magnitude. The dashed circles are to guide the eye and indicate the boundary of the base of each QD.

stack due to the larger strain magnitude there (see Fig. 2, first row for L_9).

B. Hole-wave functions exhibit atomic character

Although the electrons (lighter-mass particles) are strongly influenced by the interdot electronic and strain couplings of QDs and exhibit tunneling across the QDs forming molecular-like hybridized states, the holes due to their heavier mass remain well confined inside the individual dots and do not show any hybridization.³⁴ For example, Fig. 3 show the side views of the lowest five valence band-wave functions in the L_9 system. The horizontal dotted lines are plotted to mark the positions of the base of the QDs and helps to determine the location of a particular hole-wave function inside the stack. In this system, H_1 and H_3 are inside QD_2 , H_2 and H_5 are in QD_3 , and H_4 is in QD_8 . The location of a hole state inside

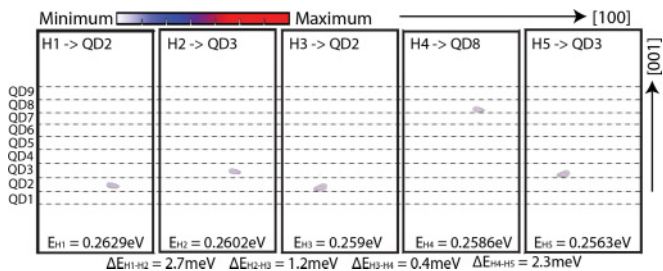


FIG. 3. (Color online) Plots of the highest five valence band states, H_1 , H_2 , H_3 , H_4 , and H_5 , for QD systems L_9 . Only the side view of the plots is shown. The horizontal dotted lines are to guide the eye and indicate the base of the QD layers in the stack. The intensity of the color in the plots indicates the magnitude of the wave function: The red color represents the highest magnitude and the light blue color represents the lowest magnitude. The energies of the valence band states and the differences between the energies of the adjacent levels are also mentioned.

a QD stack is relatively hard to determine and is strongly influenced by geometry of the QD stack, that is, QD base diameter, QD height, QD layer separation, etc. Ultimately the strain profile that controls the strength of the coupling between the QD layers inside the stack determines the position of the hole states inside the stacks.

C. Hydrostatic and biaxial strains

Figure 4 plots the hydrostatic $\epsilon_H = \epsilon_{xx} + \epsilon_{yy} + \epsilon_{zz}$ (dotted lines) and biaxial strain $\epsilon_B = \epsilon_{xx} + \epsilon_{yy} - 2\epsilon_{zz}$ (solid lines) profiles along the $[001]$ direction through the center of the QDs. The hydrostatic strain exhibits a very slight change from L_1 to L_9 . The biaxial strain, however, significantly changes as the QD stack height increases. For a single QD, L_1 ,

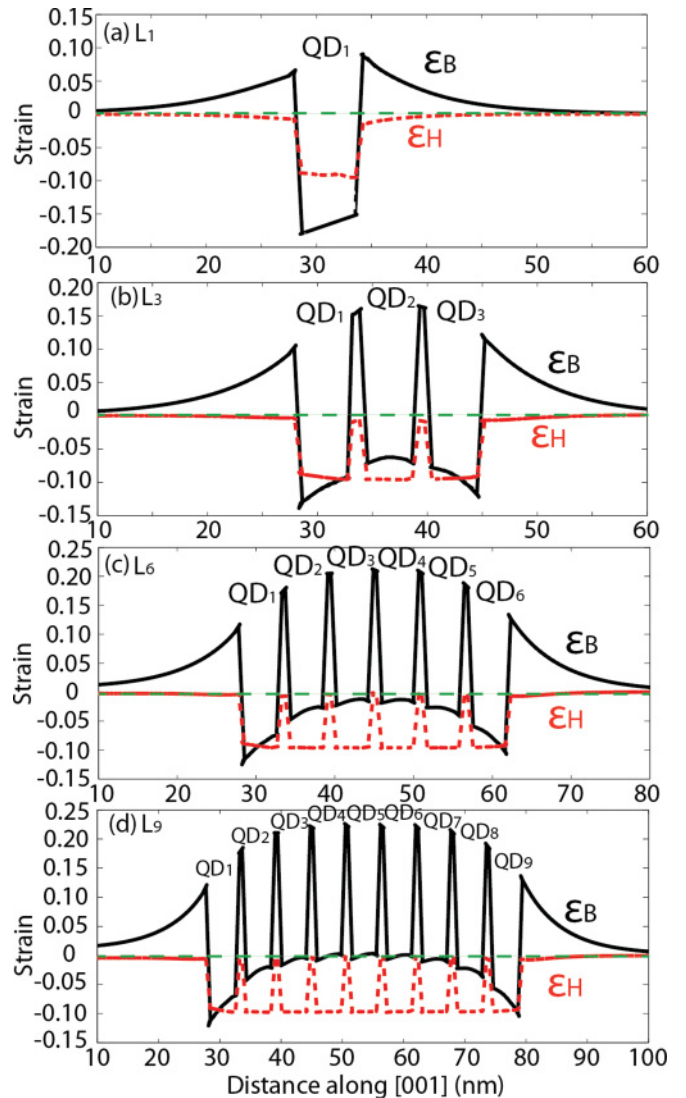


FIG. 4. (Color online) The plots of hydrostatic ($\epsilon_H = \epsilon_{xx} + \epsilon_{yy} + \epsilon_{zz}$) and biaxial strain ($\epsilon_B = \epsilon_{xx} + \epsilon_{yy} - 2\epsilon_{zz}$) components through the center of the QD system along the $[001]$ direction. The hydrostatic component is dominantly negative inside the QD, indicating strong compression of the InAs and almost zero outside the QD. As the QD stack height increases, the biaxial strain in the QD evolves from negative to zero with a small increase in positive contributions in the capping layer.

the biaxial strain is highly negative inside the QD region. As the vertical size of the QD stack is increased by adding QD layers, the biaxial strain at the center of the stack reduces. For the L_9 stack in the Fig. 4(d), the biaxial strain at the center of the stack approaches zero. The reason for such behavior of the biaxial strain is that, in general, the InAs unit cells inside the QD region tend to fit over the GaAs matrix by an in-plane compression and an elongation along the [001] direction. This results in highly negative biaxial strain as can be observed for a single QD in Fig. 4(a). However, when the size of the stack increases, the unit cells of InAs around the center of the stack feel lesser and lesser compressive force from the surrounding GaAs. As a result, the vertical lattice constant of the InAs starts matching with the GaAs and hence the biaxial strain tends to change its sign around the middle of the QD stack. Similar strain profiles were calculated in an earlier study about columnar QDs by T. Saito *et al.*²

D. Increased HH-LH mixing

The minor change in the magnitude of the hydrostatic strain (as $L_1 \rightarrow L_9$) implies that the lowest conduction band edge will experience very small change as they are only affected by the hydrostatic component.⁶ The valence band edges are affected by both the hydrostatic strain as well as the biaxial strain. The impact of strain on the highest two valence band edges, HH and LH, is analytically expressed as

$$\delta E_{HH} = a_v \epsilon_H + \frac{b_v \epsilon_B}{2}, \quad (2)$$

$$\delta E_{LH} = a_v \epsilon_H - \frac{b_v \epsilon_B}{2}. \quad (3)$$

Here a_v and b_v are deformation potential constants for HH and LH band edges. The values for these constants for InAs systems are $a_v = 1.0$ eV and $b_v = -1.8$ eV, respectively.⁶ From Eqs. (2) and (3), it is evident that the magnitude of the ϵ_B determines the HH-LH splitting. For a single QD layer, due to large negative value of ϵ_B , the HH and LH band edges will be considerably separated inside the QD region. This will induce dominant HH character in the highest few valence band states, which will be closer to the HH band edge. As the magnitude of ϵ_B decreases, the HH-LH splitting reduces, increasing the LH component in the valence band states. For the L_9 system, the nearly zero magnitude of the ϵ_B around the center of the stack implies that the HH and LH bands will be nearly degenerate around the center of the QD stack. The valence band states will therefore be of highly mixed character, consisting of contributions from both the HH and LH bands.

Figures 5(a)–5(d) plot the highest two local valence band edges, HH and LH, for all of the QD systems under study along the [001] direction through the center of the QDs. Highly negative biaxial strain in L_1 results in ~ 152 -meV splitting of HH and LH bands within the QD region. As the biaxial strain around the center of QD stack decreases (approaching toward zero), the HH-LH splitting around the center of the stack also decreases to ~ 74 , ~ 32 , and ≤ 28 meV for the L_3 , L_6 , and L_9 systems, respectively.

The HH and LH character of a particular valence band state in the tight binding formulation can be estimated as follows: If

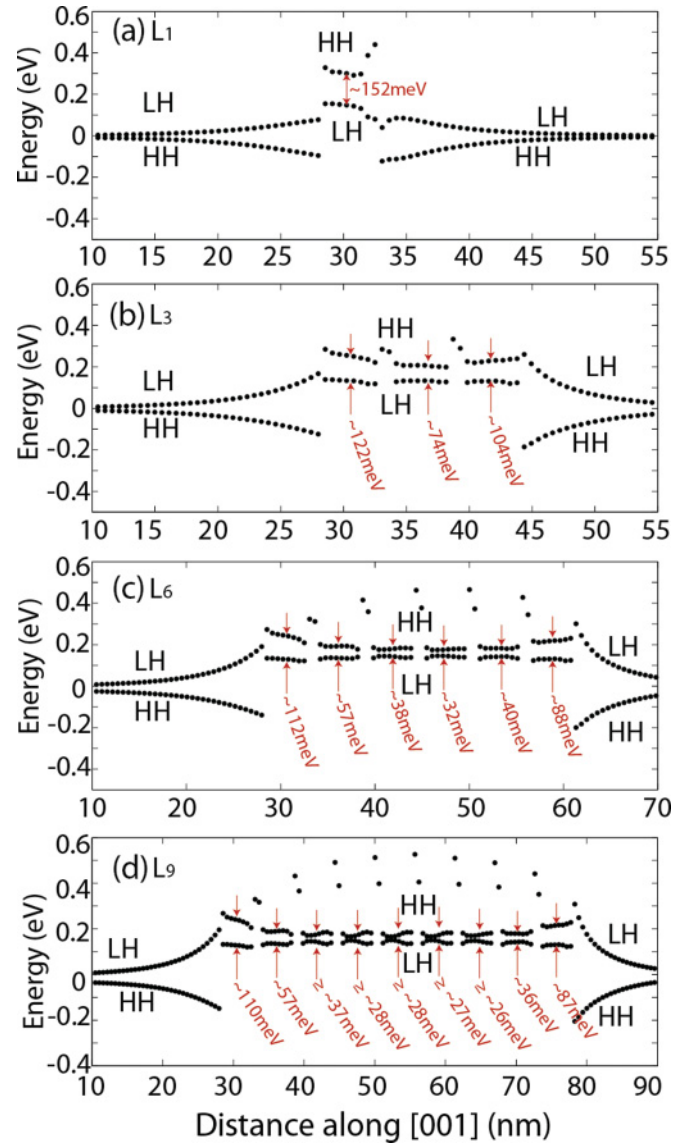


FIG. 5. (Color online) Plots of local band edges for the highest two valence bands (HH and LH) through the center of the QD along the [001] direction for L_1 , L_3 , L_6 , and L_9 . The reduction in the magnitude of biaxial strain results in larger HH/LH intermixing (lesser separation) as the size of the stack increases.

the amplitudes of the p_x , p_y , and p_z orbitals at any atomic site are $a_{x,u/d}$, $a_{y,u/d}$, and $a_{z,u/d}$, respectively (where the subscripts u and d refer to up- and down-spin), then the HH contribution is approximately proportional to $|a_{x,u} - ia_{y,u}|^2 + |a_{x,d} + ia_{y,d}|^2$ summed over all the atomic sites. The LH contribution is approximately proportional to $|a_{z,u}|^2 + |a_{z,d}|^2$ summed over all the atomic sites. By using these expressions, we estimate that the $\frac{HH}{LH}$ ratio for the highest valence band state (H_1) decreases from ~ 108 for the L_1 to ~ 15.8 , ~ 12.3 , and ~ 10.6 for the L_3 , L_6 , and L_9 systems, respectively. This clearly points toward an increasing LH character in the valence band states as the height of the QD stack increases.

E. HH/LH intermixing implies TM_{001} -mode increases

In a QD system, the HH states consist of contributions from p_x and p_y orbitals and the LH states consist of contributions

from p_x , p_y , and p_z orbitals.⁵ These configurations imply that the TM mode (which is along the z direction) will only couple to the LH states. The large splitting of the HH-LH bands [see Fig. 5(a)] resulting in a weak LH contribution in the L_1 system will result in a very weak TM_{001} mode for this system. Thus, from Eq. (1), the DOP will be nearly 1.0 and the polarization response will be highly anisotropic. As the size of the QD stack increases, the larger intermixing of HH and LH bands increases LH contribution in the valence band states. This will result in an increase of TM_{001} mode of optical transitions reducing the anisotropy of DOP, bringing it closer to 0.

F. Optical intensity functions, $f(\lambda)$

Figure 6 plots the optical intensity functions computed from our model as a function of the optical wavelength for various QD systems. The calculation of the optical intensity function is done as follows.^{10,35} First we calculate interband optical transition strengths using Fermi's golden rule by squared absolute value of the momentum matrix elements summed over spin degenerate states, $T_{E_i \rightarrow H_i} = |\langle E_i | [\vec{n}, \mathbf{H}] | H_i \rangle|^2$, where \mathbf{H} is the single-particle tight-binding Hamiltonian in the $sp^3d^5s^*$ basis, E_i and H_i are the electron and hole energy states, respectively, and \vec{n} is a vector along the polarization direction. The polarization-dependent optical modes TE_{110} , $TE_{\bar{1}10}$, and TM_{001} between the lowest conduction band state E_1 and the highest five valence band states H_1 , H_2 , H_3 , H_4 , and H_5 are calculated by rotating the polarization vector $\vec{n} = (\vec{x} + \vec{y}) \cos \phi \sin \theta + \vec{z} \cos \theta$ to the appropriate direction in the polar coordinates: For the TE_{110} mode, $\theta = 90^\circ$ and $\phi = 45^\circ$; for the $TE_{\bar{1}10}$ mode, $\theta = 90^\circ$ and $\phi = 135^\circ$; and for the TM_{001} mode, $\theta = 0^\circ$. Next each optical mode is artificially broadened by multiplication with a Gaussian distribution centered at the wavelength of the transition.^{36,37} Finally, we add all of the five Gaussian functions to calculate the total optical intensity function, $f(\lambda)$. The complete expression for the optical intensity function, plotted in Figs. 6(a)–6(k), is given by Eqs. (4) and (5):

$$f(\lambda)_{T_{E_1-H_i}} = \sum_{i=1}^5 (T^{E_1-H_i}) \cdot e^{-\frac{\lambda - \lambda_{E_1-H_i}}{(0.25)^2}}, \quad (4)$$

where

$$T^{E_1-H_i} = (TE_{110}^{E_1-H_i} / TE_{\bar{1}10}^{E_1-H_i} / TM_{001}^{E_1-H_i}). \quad (5)$$

The examination of the optical intensity plots in the Fig. 6 reveals that the TM_{001} mode indeed increases as the size of the QD stack is increased: $L_1 \rightarrow L_9$. This is, in general, true for all of the geometry configurations considered and is a direct consequence of the change in the biaxial strain component that increases HH and LH intermixing, as discussed earlier.

G. Increase in TM_{001} only partially contributes toward isotropic polarization

Figure 6 shows that the increase in the TM_{001} mode only partially helps toward an isotropic polarization response. This is in contrast to a general notion where it is described that the increase in the TM_{001} mode is mainly responsible for the

isotropic polarization. The reason for such understanding is that the previous theoretical² or the experimental studies^{1,3,11} of the DOP have assumed only one direction for the TE mode. However, our PL measurements in Figs. 1(e)–1(g) show that the TE modes along the $[110]$ and $[\bar{1}10]$ have significant anisotropy in the plane of the QD stack. The theoretical model shows that, in fact, a major contribution to achieve isotropic polarization response in these systems stems from a suppressed TE_{110} mode rather than an increased TM_{001} mode. Figure 6 shows that, irrespective of QD geometry, the increase in the TM_{001} mode is insufficient to reverse the sign of the DOP_{110} ($+ \rightarrow -$).

The TE mode is highly anisotropic in the plane of the QD with the magnitudes of the TE_{110} and $TE_{\bar{1}10}$ modes becoming very different as the QD stack size increases. For a single QD system, L_1 , $TE_{110} \sim TE_{\bar{1}10}$, and TM_{001} is very weak. Hence, the measured and calculated DOP is highly anisotropic (close to 1.0) irrespective of the direction for the TE mode. As the QD stack size increases, the TM_{001} mode also increases, partially contributing to reduction in the DOP. However, at the same time, the TE_{110} mode decreases considerably such that for L_6 and L_9 , it becomes smaller than the TM_{001} mode. The reason for such a drastic decrease in the TE_{110} mode is the orientation of hole-wave functions along the $[\bar{1}10]$ direction for the L_6 and L_9 systems.

H. Hole-wave functions are oriented along $[110]$ and $[\bar{1}10]$ resulting in $TM_{001} > TE_{110}$

Figure 7 plots the top views of the highest five valence band states H_1 , H_2 , H_3 , H_4 , and H_5 for the QD systems L_1 , L_3 , L_6 , and L_9 . The five hole-wave functions for the L_1 system have an almost uniform distribution inside the QD region with nearly symmetric shape. Such symmetry will result in approximately equal magnitude of TE mode along the $[110]$ and $[\bar{1}10]$ directions, as evident in the first row of the Fig. 7. For the stacks with three, six, and nine QD layers, the distribution of the hole-wave functions is oriented along the $[110]$ or $[\bar{1}10]$ directions. This $[110]/[\bar{1}10]$ symmetry is mainly due to the strain and piezoelectric potentials that lower the overall symmetry of the QD system and favor these two directions.^{6,34} To verify the impact of the strain and piezoelectricity, if we conduct a numerical experiment and switch off their contributions in the electronic structure calculations, the $TE_{\bar{1}10}/TE_{110}$ ratio for the L_6 system decreases from 10.92 to 0.85 and it decreases from 10.73 to 3.2 for the L_9 system. Similar distributions of the hole-wave functions are observed for bilayers¹⁰ and a single QD layer with aspect ratio³⁸ $(H/B) \geq 0.25$.

The orientation of the hole-wave functions determines the magnitude of the TE_{110} and $TE_{\bar{1}10}$ modes since the lowest electron wave function (see Fig. 2) is symmetrically distributed. For L_3 , the hole-wave functions H_1 , H_2 , and H_5 are oriented along the $[\bar{1}10]$ direction, while the other two hole-wave functions H_3 and H_4 are oriented along the $[110]$ direction. The orthogonal distributions of the hole-wave functions in L_3 will result in similar $[110]$ and $[\bar{1}10]$ TE modes. The cumulative summations for the TE_{110} and $TE_{\bar{1}10}$ modes

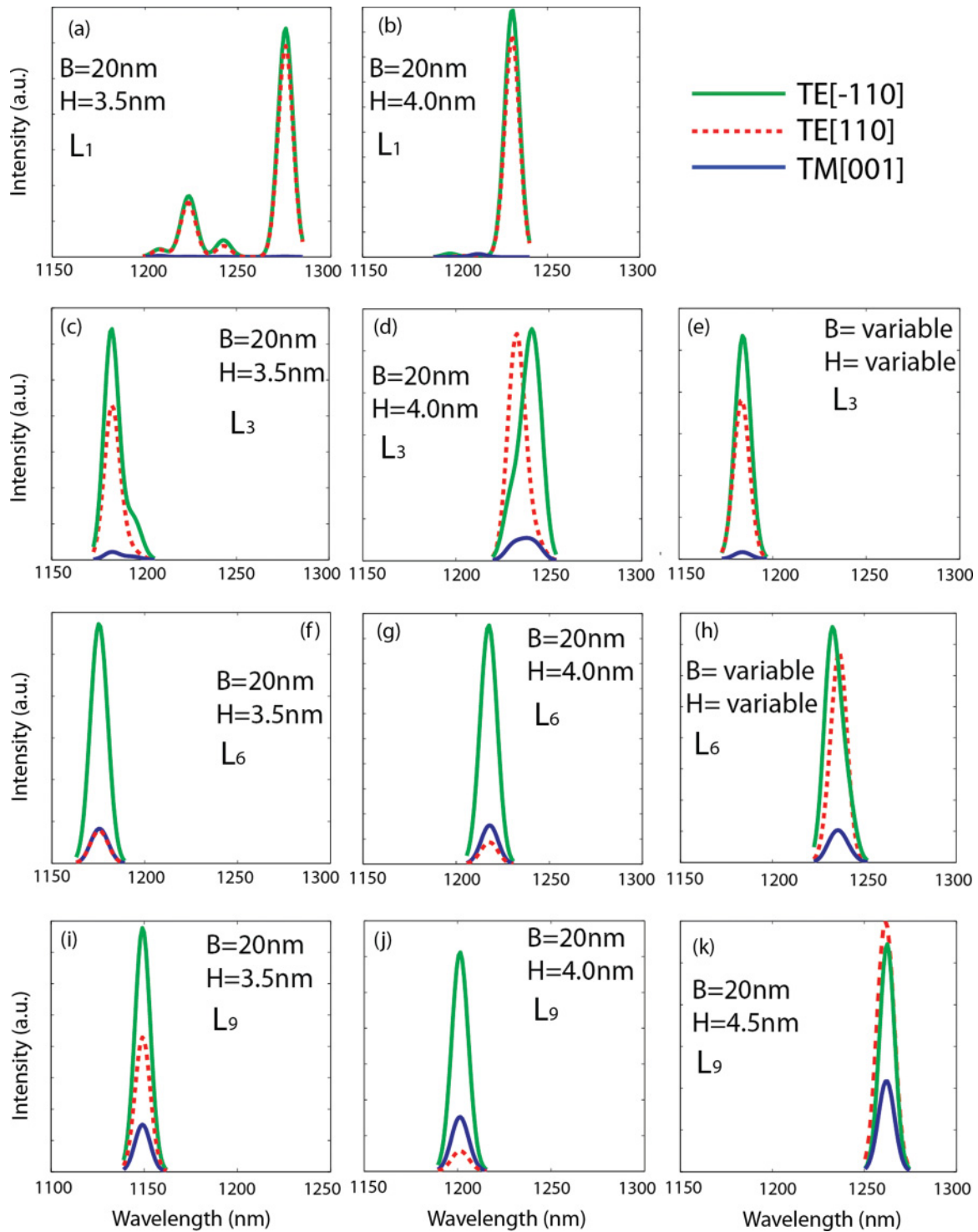


FIG. 6. (Color online) The plots of optical intensity functions, $f(\lambda)$, are shown for various QD systems. The optical intensity functions in each case are computed from Eqs. (4) and (5). The rows of the figure represent the QD system: first row, L_1 ; second row, L_3 ; third row, L_6 ; and fourth row, L_9 . The columns of the figure represent the geometry of the particular system. The first and second columns show results for identical QD stacks with 3.5- and 4.0-nm QD heights, respectively, and 20-nm base diameter. The third column is a special case where we consider increasing size of QDs for L_3 and L_6 systems. For L_9 , we again simulate identical QDs, but each with height 4.5 nm. This is the case when regular QD stack approaches columnar QD shape.

arising from these five hole states are indeed nearly equal, with $TE_{\bar{1}10}$ magnitude being slightly larger, as can be seen in Fig. 6(d).

All of the highest five hole-wave functions are oriented along the $[\bar{1}10]$ direction in the cases of the L_6 and L_9 systems. This results in a strong reduction of the TE_{110}

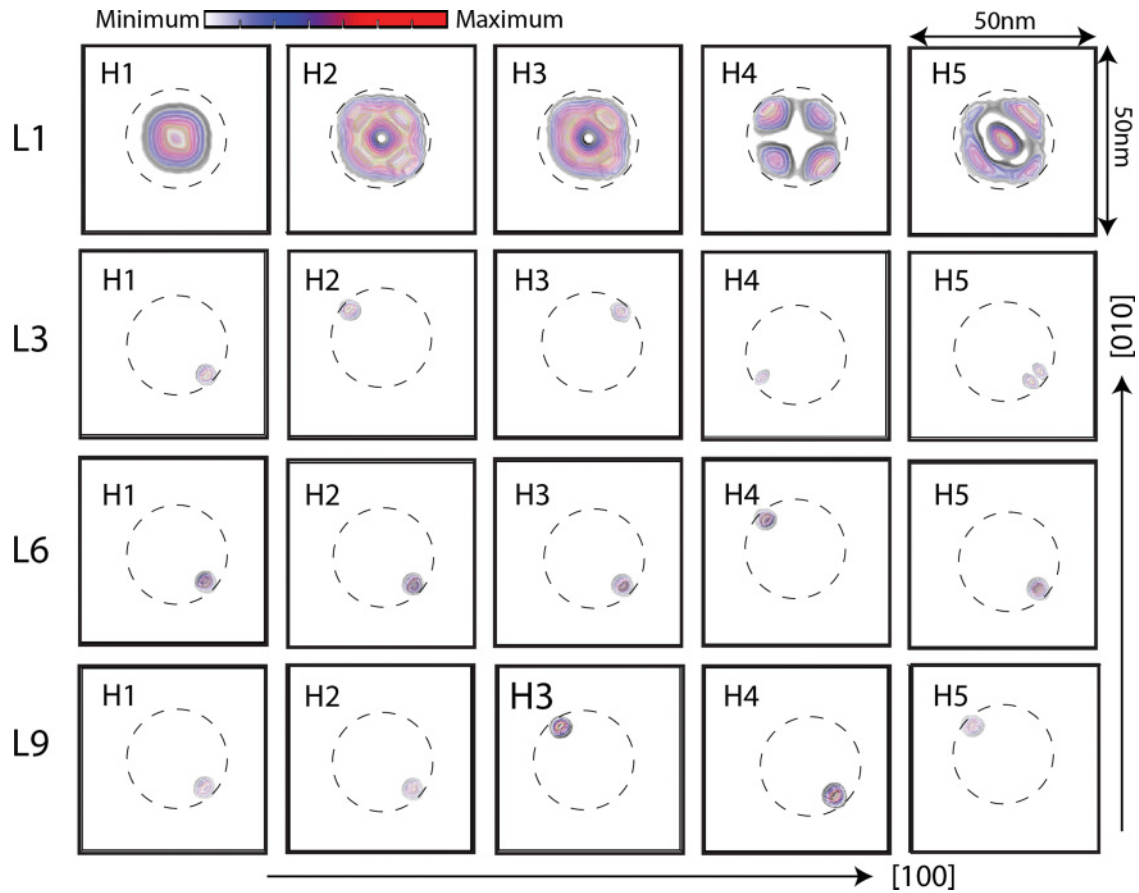


FIG. 7. (Color online) Top view of the plots of the highest five valence band states H_1 , H_2 , H_3 , H_4 , and H_5 are shown for L_1 , L_3 , L_6 , and L_9 systems. The intensity of the color indicates the magnitude of the hole-wave functions, the red color indicating the largest magnitude and the light blue color indicating the smallest magnitude. The dashed circles are to guide the eye and indicate the boundary of the QD bases.

mode. The significant reduction in the TE_{110} mode turns out to be even smaller than the magnitude of TM_{001} mode, as can be seen in the Figs. 6(f), 6(g), and 6(j). This change in relative magnitude results in a flip of sign ($+$ \rightarrow $-$) for DOP_{110} , as indeed measured in the experiment.³ Hence, we conclude that the isotropic polarization response demonstrated by the experiment is a result of two factors: (i) increase in the TM_{001} mode due to enhanced HH-LH intermixing and (ii) the reduction of TE_{110} mode due to orientation of holes along the $[\bar{1}10]$ direction.

Here we want to point out that the relative magnitude of the $TE_{\bar{1}10}$ mode does not reduce as the size of the QD stack is increased. Even for the largest system under study, L_9 , the $TE_{\bar{1}10}$ mode is much stronger than the TM_{001} mode. That means if the experimental measurements are performed for $DOP_{\bar{1}10}$, they should still show anisotropy. This is verified by our PL measurements on L_9 system shown in Fig. 1(f). These PL measurements on L_9 system indicate a positive value for the $DOP_{\bar{1}10}$ ($TE_{\bar{1}10} > TM_{001}$) and a negative value for the DOP_{110} ($TE_{110} < TM_{001}$).

I. Comparison with experimental PL data

Table I summarizes the calculated values of DOP from our model along different directions and compares it with the experimental PL measurements. Here we provide theoretically

calculated values of DOP along $[100]$ and $[010]$ directions for comparison purposes because some recent experimental studies have chosen these directions for investigation of the DOP and characterization of the polarization response of the QD systems.^{2,4,11}

The hole state symmetries shown in the Fig. 7 show strong alignment in the $[110]$ and $[\bar{1}10]$ directions, indicating that symmetries to the $[100]$ and $[010]$ directions will be almost equivalent. Therefore, the values of the DOP are nearly equal for the $[100]$ and $[010]$ directions as mentioned in the Table I. The PL measurements along these two directions will not exhibit isotropic polarization even for the L_9 system. Similar results were found in an earlier experimental study by P. Ridha *et al.*⁴ In their study of the polarization properties of multilayer stacks based on TE_{010} mode they conclude that such systems cannot provide isotropic polarization and columnar QDs are the only choice.

For the system L_1 containing only a single QD layer, our calculated DOP values in all the directions are very close to 1.0, exhibiting a very strong polarization anisotropy (TE mode \gg TM mode). The experimentally measured values for this system are relatively low (~ 0.7), but they also show that the value of the DOP remains nearly the same irrespective of the measurement direction. While the reason for difference between our calculated value and the measured value for this QD system is not very clear, other theoretical studies using the

k · p method^{2,39} on single QD layers with similar dimensions have also presented the values of the DOP close to 1.0.

J. Sensitivity of the DOP with the QD stack geometry parameters

In this section, we aim to provide theoretical guidance to the experimentalists by analyzing the dependence of the DOP on geometry parameters such as the size of QDs and the separation between the QD layers inside the QD stacks.

K. Impact of QD size on the DOP

Since the heights of the QDs in the experimental TEM images are not very clear [see Fig. 1(a)], so we simulate various geometry configurations of the QD stacks and provide the values of the DOP in the Table I. These data serve as a measure of the sensitivity of the DOP with respect to the QD stack geometry parameters and provide a guide to experimentalists to explore the design space of such complex multimillion atom systems. From the Table I, as the QD stack height increases in the $L_1 \rightarrow L_3 \rightarrow L_6 \rightarrow L_9$, the value of the DOP reduces. The reduction in the value of the DOP is larger for the stacks with $H = 4.0$ nm as compared to the stacks with $H = 3.5$ nm. This is due to the fact that the larger height of QDs in the stack results in stronger coupling between the QDs. This implies a stronger HH-LH intermixing resulting in larger magnitude of the TM_{001} mode.

The dependence of the DOP on the height (H) of the QDs inside the stacks is an unknown factor. The calculated values of the DOP in the Table I show that the DOP becomes very sensitive to the height of the QDs inside the stack as the size of the stack grows larger. For the systems L_1 and L_3 , the increase in the height (H) from 3.5 to 4.0 nm results in a small decrease in the values of the DOP. However, for a same change in the value of H , the DOP_{110} significantly decreases from 0 to -0.244 and from 0.445 to -0.45 for the

L_6 and L_9 systems, respectively. This implies that an isotropic polarization response ($DOP \sim 0$) can either be achieved from the L_6 stack with $H = 3.5$ nm, or from a stack with a fewer number of QD layers and $H = 4.0$ nm. We therefore propose that the polarization response of the QD stacks can be tuned by not only increasing the number of QD layers (a parameter tuned in the past experimental studies^{1-4,8}), but also by controlling the height (H) of the individual QDs inside the stacks.

The calculations on the L_3 and L_6 systems, where the size of QDs is increased as the stack size increases, indicate that such stacks with nonidentical QD layers will exhibit relatively higher values of the DOP and hence will not be suitable for isotropic polarization response. The same is true for the case when the height of the QDs in the L_9 system is increased to 4.5 nm such that the adjacent QD layers touch each other (approaches columnar QD limit). Based on the comparison of the calculated and the measured values of the DOP for the L_9 system in the Table I, we estimate that the dimensions of the QDs inside the stacks are approximately $B = 20$ nm and $H = 4$ nm.

L. Impact of the separation between the QD layers on the DOP

Another design parameter is the separation between the adjacent wetting layers inside the stacks. In our simulations, we have chosen a value of 4.5 nm for this parameter, which has been optimized in the self-assembly growth procedure to obtain uniform vertical stacks.¹⁷ This separation between the wetting layers results in very strong coupling of QDs and hence the electron states are hybridized over all the QDs with in the stacks as shown earlier in Fig. 2. However, if the separation between the wetting layers is increased, the coupling between the QDs will become weak and the hybridized electron states will transform to atomic-like states confined inside individual QD layers. This implies that each layer inside the multilayer

TABLE I. Comparison of experimentally measured and theoretically calculated DOP for various in-plane TE-mode directions and QD geometry configurations. Column 1, the multilayer QD system under study. Column 2, the dimensions of the QDs in the stacks. B is base diameter and H is the height of the QD. (V, V) indicates that the QDs are of varying size, base increasing by 1 nm and height increasing by 0.25 nm as the size of stack increases in the vertical direction. Columns 3–6: the values of the DOP calculated from our model. We provide two additional directions for DOP, [100] and [010], for the comparison purpose. Columns 7 and 8: the values of DOP computed from experimentally measured TE and TM modes presented in the Figs. 1(b)–1(g) or taken from T. Inoue *et al.*³

QD geometry		Theoretical calculations				Experiment	
L_N	(B, H) (nm)	DOP_{100}	DOP_{010}	DOP_{110}	$DOP_{\bar{1}10}$	DOP_{110}	$DOP_{\bar{1}10}$
L_1	(20, 3.5)	0.995	0.996	0.996	0.996	0.7	0.71
	(20, 4.0)	0.999	0.999	0.999	0.999		
L_3	(20, 3.5)	0.922	0.884	0.9046	0.933	0.67 ³	
	(20, 4.0)	0.77	0.77	0.833	0.836		
	(V, V)	0.929	0.929	0.916	0.94		
L_6	(20, 3.5)	0.594	0.594	0	0.747	0.46 ³	
	(20, 4.0)	0.548	0.46	-0.244	0.72		
	(V, V)	0.733	0.733	0.73	0.76		
L_9	(20, 3.5)	0.6	0.6	0.445	0.652	$-0.6^3, -0.36$	0.66
	(20, 4.0)	0.38	0.371	-0.45	0.603		
	(20, 4.5)	0.45	0.446	-0.47	0.43		

QD stack will behave like an independent single layer and therefore the polarization response of the multilayer QD stacks will resemble to that of the single QD layer, L_1 .

To investigate the impact of wetting layer-to-layer separation on the DOP, we increase its value from 4.5 to 7.5 nm in the L_3 , L_6 , and L_9 systems. With this new setup, we calculate following values for the DOP: for L_3 , $DOP_{110} = DOP_{\bar{1}10} = 0.973$, $DOP_{100} = DOP_{010} = 0.975$; for L_6 , $DOP_{110} = DOP_{\bar{1}10} = 0.972$, $DOP_{100} = DOP_{010} = 0.969$; and for L_9 , $DOP_{110} = 0.962$, $DOP_{\bar{1}10} = 0.968$, $DOP_{100} = DOP_{010} = 0.965$. These calculated values of the DOP clearly show that with 7.5 nm wetting layer-to-layer separation, the coupling between the QD layers is very weak and each QD inside the stack behaves like an independent layer. From these results, we conclude that a strong coupling between the QDs is critical to achieve polarization-insensitive response from the multilayer QD stacks. Further investigations of the impact of the QD geometry parameters on the DOP are being done and will be presented in our future work.

V. RESULTS AND DISCUSSIONS

This article presents a detailed analysis of the polarization response of the multilayer QD stacks by PL measurements and through a set of systematic multimillion atom tight-binding electronic structure calculations. Our theoretical results follow the trends of the experimental measurements on QD stacks containing single, three, six, and nine QD layers and provide significant physical insight of the complex physics involved

by analyzing the strain profiles, the band edge diagrams, and the wave function plots. The experimentally measured PL data for the nine-QD stack reveals a unique property by indicating a significant difference in the DOP for the $[110]$ and $[\bar{1}10]$ directions. We explain here that this difference is due to the orientation of the hole-wave functions along the $[\bar{1}10]$ direction that results in significant reduction of the TE mode along the $[110]$ direction. We suggest that the isotropic polarization response from the multilayer QD stacks is due to two factors: (i) the reduction of the TE_{110} -mode direction and (ii) the increase in the TM_{001} mode due to enhanced LH-HH intermixing. Our results presented in this paper for various geometry configurations serve as guidance for the experimentalists to design future QD-based optical devices. A flip of sign for the DOP in our PL measurements and theoretical calculations as the size of QD stack increases indicates significant potential to achieve polarization-insensitive response from multilayer QD-stack systems.

ACKNOWLEDGMENTS

Muhammad Usman gratefully thanks Susannah Heck (OCLARO, UK) for useful discussions about the polarization response of the QD samples. Computational resources accessed through the nanoHUB.org application WORKSPACE operated by the NSF funded Network for Computational Nanotechnology are acknowledged. The back-end supercomputers are operated by the Rosen Center for Advanced Computing (RCAC), Purdue University.

*usman@alumni.purdue.edu

¹P. Ridha, H. Li, M. Mexis, P. M. Smowton, J. Andrzejewski, G. Sek, J. Misiewicz, E. P. O'Reilly, G. Patriarchi, and A. Fiore, *IEEE J. Quantum Electron.* **46**, 197 (2010).

²T. Saito, H. Ebe, Y. Arakawa, T. Kakitsuka, and M. Sugawara, *Phys. Rev. B* **77**, 195318 (2008).

³T. Inoue, M. Asada, N. Yasuoka, O. Kojima, T. Kita, and O. Wada, *Appl. Phys. Lett.* **96**, 211906 (2010).

⁴P. Ridha, L. Li, M. Rossetti, G. Patriarche, and A. Fiore, *Opt. Quantum Electron.* **40**, 239 (2008).

⁵J. Singh, *Semiconductor Optoelectronics* (McGraw-Hill, New York, 1995).

⁶M. Usman, H. Ryu, I. Woo, D. S. Ebert, and G. Klimeck, *IEEE Trans. Nanotechnol.* **8**, 330 (2009).

⁷J. Tatebayashi, N. Nishioka, and Y. Arakawa, *Appl. Phys. Lett.* **78**, 3469 (2001).

⁸T. Kita, O. Wada, H. Ebe, Y. Nakata, and M. Sugawara, *Jpn. J. Appl. Phys., Part 2* **41**, L1143 (2002).

⁹T. Kita, N. Tamura, O. Wada, M. Sugawara, Y. Nakata, H. Ebe, and Y. Arakawa, *Appl. Phys. Lett.* **88**, 211106 (2006).

¹⁰M. Usman, S. Heck, E. Clarke, P. Spencer, H. Ryu, R. Murray, and G. Klimeck, *J. Appl. Phys.* **109**, 104510 (2011).

¹¹L. Fortunato, M. T. Todaro, V. Tasco, M. De Giorgi, M. De Vittori, R. Cingolani, and A. Passaseo, *Superlattices Microstruct.* **47**, 72 (2010).

¹²O. Kojima, H. Nakatani, T. Kita, O. Wada, K. Akahane, and M. Tsuchiya, *J. Appl. Phys.* **103**, 113504 (2008).

¹³O. Kojima, H. Nakatani, T. Kita, O. Wada, and K. Akahane, *J. Appl. Phys.* **107**, 073506 (2010).

¹⁴M. Richter, M. Damilano, B. Duboz, J.-Y. Massies, and J. Wieck, *Appl. Phys. Lett.* **88**, 231902 (2006).

¹⁵J. Jiang, S. Tsao, T. O'Sullivan, W. Zhang, H. Lim, T. Sills, K. Mi, M. Razeghi, G. J. Brown, and M. Z. Tidrow, *Appl. Phys. Lett.* **84**, 2166 (2004).

¹⁶H. Liu, M. J. Steer, T. J. Badcock, D. J. Mowbray, M. S. Skolnick, P. Navaretti, K. M. Groom, M. Hopkinson, and R. A. Hogg, *Appl. Phys. Lett.* **86**, 143108 (2005).

¹⁷T. Inoue, M. Asada, O. Kojima, T. Kita, and O. Wada, *Proc. SPIE* **7597**, 75971J (2010).

¹⁸T. Inoue, M. Asada, N. Yasuoka, T. Kita, and O. Wada, *J. Phys.: Conf. Ser.* **245**, 0120761 (2010).

¹⁹Y. Ikeuchi, T. Inoue, M. Asada, Y. Harada, T. Kita, E. Taguchi, and H. Yasuda, *Appl. Phys. Express* **4**, 062001 (2011).

²⁰P. Podemski, G. Sek, K. Ryczko, J. Misiewicz, S. Hein, S. Hoffing, A. Forchel, and G. Patriarche, *Appl. Phys. Lett.* **93**, 171910 (2008).

²¹G. Klimeck, S. Ahmed, H. Bae, N. Kharche, R. Rahman, S. Clark, B. Haley, S. Lee, M. Naumov, H. Ryu, F. Saied, M. Parada, M. Korkusinski, and T. B. Boykin, *IEEE Trans. Electron Devices* **54**, 2079 (2007).

²²G. Klimeck, S. Ahmed, N. Kharche, M. Korkusinski, M. Usman, M. Parada, and T. B. Boykin, *IEEE Trans. Electron Devices* **54**, 2090 (2007).

²³P. Keating, *Phys. Rev.* **145**, 637 (1966).

- ²⁴L. O. Lazarenkova, P. von Allmen, O. Fabiano, L. Seungwon, and G. Klimeck, *Appl. Phys. Lett.* **85**, 4193 (2004).
- ²⁵T. B. Boykin, G. Klimeck, R. C. Bowen, and F. Oyafuso, *Phys. Rev. B* **66**, 125207 (2002).
- ²⁶S. Ahmed, N. Kharche, R. Rahman, M. Usman, S. Lee, H. Ryu, H. Bae, S. Clark, B. Haley, M. Naumov, F. Saied, M. Korkusinski, R. Kennel, M. McLennan, T. B. Boykin, and G. Klimeck, e-print [arXiv:0901.1890](https://arxiv.org/abs/0901.1890) (to be published).
- ²⁷M. Usman, S. Ahmed, and G. Klimeck, *Proceedings of the 8th IEEE Conference on Nanotechnology* (IEEE, Arlington, TX, 2008), pp. 541–544.
- ²⁸M. Korkusinski and G. Klimeck, *J. Phys.: Conf. Ser.* **38**, 75 (2006).
- ²⁹N. Kharche, M. Parada, T. B. Boykin, and G. Klimeck, *Appl. Phys. Lett.* **90**, 092109 (2007).
- ³⁰R. Rahman, C. J. Wellard, F. R. Bradbury, M. Parada, J. H. Cole, G. Klimeck, and L. C. L. Hollenberg, *Phys. Rev. Lett.* **99**, 036403 (2007).
- ³¹M. Usman, C. A. Broderick, A. Lindsay, and E. P. O'Reilly, *Phys. Rev. B* (in press).
- ³²Q. Xie, A. Madhukar, P. Chen, and N. P. Kobayashi, *Phys. Rev. Lett.* **75**, 2542 (1995).
- ³³S. Lee, J. Kim, L. Jonsson, J. W. Wilkins, G. W. Bryant, and G. Klimeck, *Phys. Rev. B* **66**, 235307 (2002).
- ³⁴G. Bester and A. Zunger, *Phys. Rev. B* **72**, 165334 (2005).
- ³⁵M. Usman, Y.-H. Matthias Tan, H. Ryu, S. S. Ahmed, H. J. Krenner, T. B. Boykin, and G. Klimeck, *Nanotechnology* **22**, 315709 (2011).
- ³⁶O. Stier, M. Grundmann, and D. Bimberg, *Phys. Rev. B* **59**, 5688 (1999 II).
- ³⁷Y.-Y. Lin and J. Singh, *J. Appl. Phys.* **92**, 6205 (2002).
- ³⁸M. Usman, *J. Appl. Phys.* (in press).
- ³⁹W. Sheng and J.-P. Leburton, *Appl. Phys. Lett.* **80**, 2755 (2002).